

Molecular dynamics simulations of viral neuraminidase inhibitors with the human neuraminidase enzymes: Insights into isoenzyme selectivity

Michele R. Richards, Tianlin Guo, Carmanah D. Hunter, Christopher W. Cairo*

*Alberta Glycomics Centre and Department of Chemistry, University of Alberta, Edmonton, AB
T6G 2G2, Canada*

Dedicated to Professor Laura L. Kiessling on the receipt of the 2017 Tetrahedron Prize

*Correspondence, Tel.: 780 492 0377; fax: 780 492 8231; e-mail: ccairo@ualberta.ca

Abstract:

Inhibitors of viral neuraminidase enzymes have been previously developed as therapeutics. Humans can express multiple forms of neuraminidase enzymes (NEU1, NEU2, NEU3, NEU4) that share a similar active site and enzymatic mechanism with their viral counterparts. Using a panel of purified human neuraminidase enzymes, we tested the inhibitory activity of 2-deoxy-2,3-dehydro-*N*-acetylneuraminic acid (DANA), zanamivir, oseltamivir, and peramivir against each of the human isoenzymes. We find that, with the exceptions of DANA and zanamivir, these compounds show generally poor activity against the human neuraminidase enzymes. To provide insight into the interactions of viral inhibitors with human neuraminidases, we conducted molecular dynamics simulations using homology models based on coordinates reported for NEU2. Simulations revealed that an organized water is displaced by zanamivir in binding to NEU2 and NEU3 and confirmed the critical importance of engaging the binding pocket of the C7–C9 glycerol sidechain. Our results suggest that compounds designed to target the human neuraminidases should provide more selective tools for interrogating these enzymes. Furthermore, they emphasize a need for additional structural data to enable structure-based drug design in these systems.

1 Introduction

Sialic acids, also known as neuraminic acids, are α -keto nonulosonic acids that are typically the terminal carbohydrate of glycoproteins and glycolipids.¹ The most common sialic acid in humans is *N*-acetylneuraminic acid (Neu5Ac **1**, **Figure 1**), though other forms are known.² Due to their placement at the periphery of the glycan, sialic acids act as receptors for pathogens, as well as signaling molecules for the immune system,¹ and their expression is controlled by the interplay of sialyltransferases (SiaTs) and neuraminidase enzymes (NEUs).³ Four human neuraminidases (hNEUs) have been identified: NEU1, NEU2, NEU3, and NEU4.⁴ The expression of hNEUs has been linked to cancer, diabetes, and cardiovascular disease.⁵⁻⁷ Human NEUs may play roles in inflammation through modification of the sialyl-Lewis_x (CD15s) antigen on leukocytes.^{8, 9} Although a variety of studies have been conducted using biological models where hNEUs have been disrupted by genetic methods,^{4, 6} the availability of competitive inhibitors for these enzymes should provide important tools to reveal the role of individual isoenzymes in disease and could form the basis of new therapeutic strategies.¹⁰

Inhibitors of influenza NEU form the basis of clinically available antiviral therapeutics;¹¹ however, these inhibitors may not be generally active against NEUs from different species. Most NEU inhibitors are based on 2-deoxy-2,3-dehydro-*N*-acetylneuraminic acid (DANA, **2**) as a parent structure. Zanamivir **3** and oseltamivir **4**, analogs of DANA originally designed to target influenza A neuraminidase, are also active against NanA from *Streptococcus pneumoniae*, with IC₅₀ values reported in the low micromolar range.¹² An analysis of multiple NanA sequences suggested that oseltamivir has broad activity against bacterial NEUs.¹³ Cross species viral–bacterial NEU inhibition could play a role in the severity of influenza infections, and inhibitors with activity against NEUs from both species could provide clinical benefit.¹⁴ If viral NEU (vNEU) inhibitors

have broad specificity for bacterial species, one might expect the same is true for hNEUs. However, studies that have examined the activity of oseltamivir and zanamivir against hNEUs have generally observed substantially weaker potency against these enzymes, typically observing high micromolar to low millimolar IC_{50} values. Hata et al. found that oseltamivir had low millimolar inhibition of NEU2, as did zanamivir for NEU1, NEU2, and NEU4. In contrast, zanamivir had low micromolar activity against the NEU3 isoenzyme.¹⁵ Chavas et al. observed mid-to-high micromolar activity for zanamivir and peramivir (**5**) with NEU2, but oseltamivir showed very low activity.¹⁶ Analogs of oseltamivir tested against NEU3 and NEU4 showed generally low activity and suggested an important role for the C7–C9 glycerol side-chain of Neu5Ac in enzyme recognition.¹⁷ Despite low in vitro inhibitory potency for oseltamivir with NEU1, several reports have investigated its use to block signaling pathways related to cancer, diabetes, and fibrosis linked to this isoenzyme.^{18–20} We note that subtle changes in formulation of oseltamivir can show significant variations in activity in cell-based assays.²¹ It has been previously suggested that mutations in hNEUs could make individuals more susceptible to adverse effects of antiviral medications.²² The de-sialylation of platelets is a major mechanism of cell clearance in transfusions, and hNEUs also appear to be involved in senescence and autoimmune mechanisms of platelet clearance.^{23, 24} Inhibitors of NEU have been investigated for enhancement of platelet storage by targeting NEU from contaminating bacteria.²⁵

While inhibitors optimized to act as antivirals show weaker activity against hNEUs, the design of inhibitors that specifically target these enzymes has identified important features of their binding sites.¹⁰ The development of inhibitors tailored to the human NEUs has been impeded by limited structural data on the enzymes. Of the four hNEUs, only NEU2 has been crystallized – both in its apo form and in complex with several inhibitors, including DANA, zanamivir, and

peramivir.^{16, 26} While the substrate Neu5Ac is found in a ²C₅ conformation in solution,²⁷ inhibitors **2–4** are all six-membered rings with half-chair conformations that presumably mimic the transition state of catalyzed Neu5Ac cleavage.²⁸ Magesh et al. identified that C9-amide derivatives of DANA were active against NEU1.²⁹ Our group has reported inhibitors with C9- or C4,C9-modifications are able to specifically target NEU4 and NEU3 enzymes with nanomolar potency and excellent selectivity.^{30, 31}

To expand our understanding of differences between the active sites of hNEUs and their viral counterparts, we set out to examine the activity of known viral inhibitors against a panel of human NEUs. We first developed homology models for NEU1, NEU3, and NEU4, and used these, along with the crystal structures of NEU2, as starting points for molecular dynamics (MD) simulations to provide insight into the selectivity of **3** toward NEU2 and NEU3. Furthermore, we measured the IC₅₀ and inhibitory constants (*K_i*) of compounds **1–5** against individual hNEU to provide experimental context for our models. The results of the simulations, and their relation to the design of new selective inhibitors of the four NEU isoenzymes, is described.

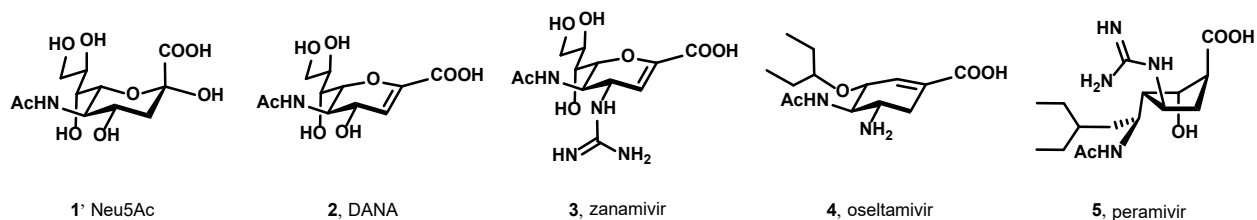


Figure 1. Compounds evaluated in this study.

2 Materials and methods

Compounds **1** and **5** were purchased from Dextra Laboratories Ltd. and Ontario Chemicals Inc., respectively, and used without further purification. Compounds **2** and **3** were synthesized as described previously.³¹ Oseltamivir phosphate was purchased from Sigma-Aldrich, and the ethyl ester was hydrolyzed with NaOH to generate the carboxylate form **4**, which was used for assays.³² See Supporting Information for details of the protocol.

2.1 K_m determinations

A sample of the enzyme (5 μ L; 0.25 mU for NEU1, 0.5 mU for NEU2 – NEU4) was incubated in a 384-well plate with reaction buffer (10 μ L; 0.1 M sodium acetate buffer) at the enzyme's optimum pH, and 4MU-NANA (5 μ L; 0–400 μ M). The rate of product formation was monitored using fluorescence ($\lambda_{\text{ex.}} = 315 \text{ nm}$ $\lambda_{\text{em.}} = 450 \text{ nm}$) every 2 minutes for 30 minutes (NEU1, NEU3, and NEU4) or every 20 seconds for 5 minutes (NEU2). Michaelis-Menten kinetics were determined from duplicate measurements using nonlinear regression in GraphPad Prism 7.0.

2.2 Inhibition assays

Human NEU2, NEU3, and NEU4 enzymes were expressed as MBP-fusion proteins in *E. coli* and purified as previously reported.^{17, 33} NEU1 was overexpressed as a (His)₆ fusion protein in HEK293 cells and used as a crude preparation from cell lysate.³⁴ All assays were conducted in 0.1 M sodium acetate buffer at optimum pH for each enzyme (pH 4.5 for NEU1, NEU3, and NEU4; pH 5.5 for NEU2).³⁵ To get comparable IC₅₀ values among the four isoenzymes, similar activity of each enzyme was used in the assay based on 4MU-NANA (4'-methylumbelliferyl α -D-N-acetylneuraminic acid) activity. Assays were performed using protocols reported previously.³⁵

Inhibitors over a concentration range of 3-fold serial dilutions were incubated with enzyme at 0 °C for 15 min. 4MU-NANA was then added to the mixture, bringing the final concentration of 4MU-NANA to 50 μ M and the total volume of the reaction mixture to 20 μ L. After incubation at 37 °C for 30 min, the reaction was quenched with 100 μ L of 0.2 M sodium glycine buffer (pH 10.2). The reaction mixture was transferred to 386-well plate and the enzyme activity was determined by measuring fluorescence ($\lambda_{\text{ex}} = 365$ nm; $\lambda_{\text{em}} = 445$ nm) using a plate reader (Molecular Devices, Sunnyvale CA). Assays were performed with duplicates for each point and IC_{50} was obtained by plotting the data with GraphPad Prism 7.0. For curves that showed less than a 50% decrease in signal, fits were conducted using the maximum inhibition values found for DANA.

2.3 *K_i determinations*

Enzymes were incubated with serial concentrations of inhibitors at 0 °C for 15 min and serial concentrations of 4MU-NANA were then added. The reaction mixture was transferred to a 384-well plate immediately and the rate of product formation was obtained by measuring fluorescence ($\lambda_{\text{ex}} = 315$ nm; $\lambda_{\text{em}} = 450$ nm) every 1 min for 30 min. The data were processed with GraphPad Prism 7.0 for K_i determination.

2.4 *Computational methodology*

2.4.1 *Enzyme models*

Molecular dynamics (MD) simulations were run for compounds **1–5** bound to the four hNEU isoenzymes. We used the crystal structure of NEU2 bound to **2** (PDB ID: 1VCU)^{26, 36} as the initial structure for NEU2 and added the missing non-terminal residues G227, E228, S284, G295, P286, and G287 using Modeller in Chimera.³⁷⁻⁴⁰ For NEU3 and NEU4, we used our

previously reported homology models.^{2, 31, 33, 41} Additionally, the model for NEU3 was modified to eliminate unreasonable conformations using Modeller in Chimera. We built a homology model for NEU1 also using Modeller in Chimera and the alignment reported by Magesh, et al.^{29, 42} The alignments for the four isoenzymes are shown in **Figure 2**. Residues 1–53 in NEU1 and 290–367 in NEU4 have no homology to NEU2 and were removed before running MD simulations.

2.4.2 Inhibitor models

The starting coordinates for the inhibitors were obtained for **1** from 4NCS,^{43, 44} for **2** from 1VCU,^{26, 36} for **3** from 2F0Z,^{16, 45} for **4** from 2QWK,^{46, 47} and for **5** from 2F10.^{16, 48} We kept the active site waters from 4NCS for simulations with **1**, from 1VCU for simulations with **2**, from 2F0Z for simulations with **3**, from 2QWK for simulations with **4**, and from 2F10 for simulations with **5**. We aligned each of the enzymes NEU1, NEU3, and NEU4 (MatchMaker in Chimera³⁸⁻⁴⁰) separately with NEU2 to obtain the initial positions for **1–5** bound to the homology models. All compounds were simulated with the protonation states at physiological pH (i.e. as carboxylate, ammonium, and/or guanidinium ions). See Supporting Information for starting structures of MD simulations in PDB format,^{49, 50} along with the files necessary for running inhibitors **2–5** in AMBER.

```

Neu1 1 M.TGERPSTA LPDRRWGPRI LGFWGGCRVW VFAAIFLLLS LAASWSKAEN DFGLVQPLVT
Neu2 1 M..... ASLPVL
Neu3 1 M..... EEVTTC
Neu4 1 M..... GVP RTP
      *

Neu1 60 MEQL.LWVSG ..RQIGSVD TFRIPPLITAT PRG.TLLAFA EARKMSSSDE GAKFIALRRS
Neu2 8 QKES.VFQSG ...A.....H AYRIPALLYL PGQQSLLAFA EQRASK.KDE HAELIVLRRG
Neu3 8 SFNSPLFRQE DDRG....I TYRIPALLYI PPTHFLAFA EKRSTR.RDE DALHLVLRG
Neu4 8 SRTV.LFERE R.TG....L TYRVPSLLPV PPGPTLLAFV EQRLSP.DDS HAHRLVLRG
      ::          ::**:* : * :***. * * * . * :***.

Neu1 115 MD.Q...GST WSPTAFIVND GDVPDGLNLG AVVSDVETGV VFLFYSL.CA HK...A...
Neu2 58 DYDAPTHQVQ WQAEVVAQA RLDGHRSMNP CPLYDAQTGT LFLFFIAIPG QVTEQQQLQT
Neu3 62 L.R.IGQLVQ WGPLKPLMEA TLPGHRTMNP CPVWEQKSGC VFLFFICVRG HVTERRQIVS
Neu4 60 TLAG..GSVR WGALHVLGTA ALAEHRSMNP CPVHDAGTGT VFLFFIAVLG HTPEAVGIAT
      * . : . . : : * :***: . :

Neu1 163 ...GCQVAST MLVWSKDDGV SWSTPRNLSL DI.GT.E... .VFAPGPGS GIQKQREPRK
Neu2 118 RANV.T..RL CQVTSTDHGR TWSSPRDLTD AAIGPAYREW ST.FAVGPGH CLQLNDR..A
Neu3 120 GRNA.A..RL CFIYSQDAGC SWSEVRDLTE EVIGSELKHW AT.FAVGPGH GIQLQS...
Neu4 118 GRNA.A..RL CCVASRDAGL SWGSARDLTE EAIGGAVQDW AT.FAVGPGH GVQLPS...
      : * * * :* * :* : * * * * :*

Neu1 213 GRLIVCGHGT LER..... DGVC LLSDDHGASW RYGGSV.SGI
Neu2 172 RSLVVPAYAY ..RK..... L.HP.....I QRPIP.SAFC FLSDHGRGW ARGHFV.A..
Neu3 172 GRLVIPAYTY ..YIPSWFFC F.QL....P CKTRP.HSLM IYSDDLGVTW HGRRLIRP..
Neu4 170 GRLLVPAYTY ..RV..... DRR.ECFGKI CRTSP.HSFA FYSDDHGRGW RCGGLVPN..
      *:: : : : * * * :* * :

Neu1 250 PYGQPKQEND FNPDECQPYE LPDG....S VVINARNQNN YHCHCRIVLR SYDACDTRLR
Neu2 214 ..... QDTLEQVAE VETGE.Q.RV VTLNARSHLR A...RVQAQ STNDGLDFQE
Neu3 221 ..... MVTVECEVAE VTGRA.GHPV LYCSARTPNR C...RAEAL STDHGEGFQR
Neu4 218 ..... LRSGEQQLAA VDGGQAG.SF LYCNARSPLG S...RVQAL STDEGTSFLP
      . ** : : : ** . * * : :

Neu1 305 RDVTFDP.E. ....LVDPVV AAG..... .AVVTS...
Neu2 258 SQLVKKLVEP PPQGCQGSVI SFP..... SP R....S...
Neu3 266 LALSRQLCEP P.HGCQGSV SFRPLEIPHR QDSSSKDAP TI....QQ.. SS.....
Neu4 263 AERVASLPET A.WGCQGSIV GFP..... AP A....P.NR PRDSSWSVGP
      . * .....

Neu1 327 .....
Neu2 285 .....
Neu3 311 .....
Neu4 301 GSPLQPPLLG PGVHEPPEEA AVDPRGGQVP GGPFSRLQPR GDGPRQPGPR PGVSGDVGSW

Neu1 327 .....S.GI VFFSNPAHPE FRVNLTLRWS ..FSNGTSWR
Neu2 285 .....GP G...S..... PAQW LLYTHPTSHW QRADLGAYLN PRPPAPEAWS
Neu3 311 ..... .PGS.SLRLE EEAGTPSESW LLYSHPTSrk QRVDLGIYLN QTPLEAACWS
Neu4 361 TLALPMPFAA P..PQ..... .SPTW LLYSHPVGRR ARLHM GIRLS QSPLDPRSWT
      . : : * . * : . *

Neu1 358 KETVQLWPGP SGYSSLATLE GSMDGEEQAP QLYVLYEKGR .NH.YTESIS VAKISVYGTL
Neu2 323 EPVLLAK.GS CAYSDLQSMG TGPD.GS..P .LFGCLYEAN ....DYEEI VFLMFTLKQA
Neu3 359 RPWILHC.GP CGYSDLAALE EE.....G .LFGCLFECG TKQ..ECEQI AFRLFTHREI
Neu4 408 EPWVIYE.GP SGYSDLASIG PAPE.GG..L .VFACLYESG ..ARTSYDEI SFCTFSLREV
      . : * . **.* : : : :

Neu1 415 .....
Neu2 373 FP.....AEY...
Neu3 408 LSHLQGDCTS PGRNP.SQFK SN
Neu4 461 LE.....NVP...

```

Figure 2. Alignment of the four hNEU isoenzymes.

2.4.3 Simulations

All simulations were run in AMBER 15⁵¹ using *pmemd.cuda* (GPU acceleration) on Nvidia GeForce GTX 980 GPUs. The *ff14SB* force field⁵² was used for the proteins, GLYCAM06 was used for **1**,⁵³ and the general AMBER force field (GAFF)⁵⁴ was used for **2–5**. Hydrogens were added to **2–4** using the program Avogadro,^{55, 56} then partial charges for **2–4** were assigned using AM1 with bond charge correction (AM1-BCC) model⁵⁷ in the *antechamber* module of AmberTools15.⁵¹ We used our previously reported parameters and charges for **5**.⁵⁸ The enzyme–inhibitor complexes were neutralized with the addition of Na⁺ ions or Cl⁻ ions as necessary, and Joung-Cheatham parameters were used for the ions.⁵⁹ All complexes were solvated in a box of TIP3P water⁶⁰ with 10 Å between the solute and the edges of the box in all three dimensions. For all systems, the water was first minimized using 100 steps of steepest descent, followed by 4900 steps of conjugate gradient. Then the entire system was minimized with 100 steps of steepest descent, followed by 4900 steps of conjugate gradient. The systems were further equilibrated by heating from 5 K to 300 K over 50 ps, followed by cooling back to 5 K over an additional 50 ps. After the annealing step, the systems were again heated from 5 K to 300 K over 100 ps, then allowed to run at 300 K for 100 ps before the production simulations were started. Production was run for 100 ns in each system. The timestep was 2 fs, bonds to hydrogen were constrained with the SHAKE⁶¹ algorithm, and the cutoff for non-bonded interactions was 8.0 Å. The temperature was maintained with the Berendsen thermostat⁶² (*ntt* = 1) with velocities rescaled every 1 ps. The simulations were analyzed using the *cpptraj* module of AmberTools15.^{51, 63}

3 Results and discussion

3.1 Activity of viral inhibitors against hNEU

Previous reports have investigated the activity of viral inhibitors with hNEU isoenzymes. In most cases, the 4MU-NANA substrate is used to allow for rapid analysis using fluorescence spectroscopy. The activity of the purified enzymes for this substrate have been reported elsewhere,¹⁵ and we sought to measure the activity of our recombinant enzymes before investigating the activity of inhibitors using 4MU-NANA as a substrate (**Table 1**). Of the four neuraminidases, NEU4 had the lowest measured K_m of 17 ± 2 μM . We observed a K_m of 48 ± 9 μM for NEU3, in agreement with previous data.^{33, 64} These results are in contrast to studies using overexpressed sources of hNEU isoenzymes; which observed much higher K_m values for NEU1 and NEU2.¹⁵ We note that previous work with our recombinant enzyme preparations have found good agreement between their activity and enzymes from eukaryotic cells.^{31, 65} It is interesting to note that the activity of NEU4 for the 4MU-NANA substrate has been consistently found to be higher than the other isoenzymes, suggesting some substrate preference for the 4-methylumbulliferyl aglycone.^{2, 15} The NEU2, NEU3, and NEU4 isoenzymes are reported to modify glycolipid substrates to varying degrees, in contrast to NEU1 which generally prefers glycoproteins.^{66, 67} Our data suggest that 4MU-NANA shows similar K_m values for all four isoenzymes, which should allow for comparison of inhibition assay data using this substrate.

Table 1. K_m values of 4MU-NANA against hNEUs

Enzyme	K_m (μM) ^a
NEU1	56 ± 18
NEU2	119 ± 21
NEU3	48 ± 9
NEU4	17 ± 2

^a Error shown is standard error calculated from nonlinear regression.

Testing of compounds **1–5** for inhibitor activity against hNEU was performed with 4MU-NANA as the substrate to determine IC_{50} (**Table 2**) and K_i values (**Table 3**). We observed that NEU1 had undetectable inhibition from all compounds tested, with the exception of **2**, which had an IC_{50} of $49 \pm 8 \mu\text{M}$ (K_i of $12 \pm 1 \mu\text{M}$). Compound **2** was the only compound which had activity against all four isoenzymes, ranging from 8–50 μM .³¹ The monosaccharide, Neu5Ac **1**, had undetectable inhibition of all four isoenzymes; as did oseltamivir **4**. Peramivir **5** only had detectable inhibition against NEU2 (IC_{50} of $70 \pm 7 \mu\text{M}$; K_i of $56 \pm 13 \mu\text{M}$) and was inactive against all other isoenzymes. Previous reports have observed higher K_i values for peramivir **5** with NEU2.¹⁶ Zanamivir **3** was the most potent compound tested and showed activity against NEU2, NEU3, and NEU4 consistent with previous reports.^{15, 16, 31} Zanamivir had sub-micromolar activity against NEU3 (K_i $0.62 \pm 0.09 \mu\text{M}$) but only had low micromolar activity against NEU2 and NEU4. These inhibition data suggest that the only viral NEU inhibitor tested with notable activity against hNEU isoenzymes was zanamivir. We have previously identified 4-guanidino analogs of DANA as selective inhibitors of NEU3 when combined with modifications at the C9 position.³¹ Additionally, these data are consistent with previous investigations of oseltamivir analogs with hNEU, which found that replacement of the amino group of **4** with a guanidine was insufficient to improve activity of these compounds against NEU3 and NEU4 isoenzymes.¹⁷ In earlier analysis of the conformation of peramivir in solution and in viral enzyme active sites, we observed large changes in ring conformation.⁵⁸ Based on our results here, we sought to re-evaluate the binding of viral compounds to models of the hNEU isoenzymes using molecular modeling.

Table 2. IC₅₀ (μM) values^a for **1–5** against hNEUs

Compound	NEU1	NEU2	NEU3	NEU4
1 - Neu5Ac	>500	>500	>500	>500
2 - DANA	49 ± 8	37 ± 6	7.7 ± 0.8	8.3 ± 1.0
3 - Zanamivir	>500	7.8 ± 2.0	4.0 ± 0.6	47 ± 6
4 - Oseltamivir	>500	>500	>500	>500
5 - Peramivir	>500	70 ± 7	>500	>500

^a **Error shown is standard error calculated from nonlinear regression.** **Table 3.** K_i (μM) values^a for inhibitors **1–5** against hNEUs

Compound	NEU1	NEU2	NEU3	NEU4
1 - Neu5Ac	NA	NA	NA	NA
2 - DANA	12 ± 1	25 ± 4	1.6 ± 0.3	5.8 ± 0.6
3 - Zanamivir	NA	5.7 ± 1.5	0.62 ± 0.09	26 ± 4
4 - Oseltamivir	NA	NA	NA	NA
5 - Peramivir	NA	56 ± 13	NA	NA

^a Error shown is standard error calculated from nonlinear regression.

3.2 MD simulations of hNEUs with viral inhibitors

There is limited structural data for the hNEU enzymes, with crystal structures only having been reported for NEU2,^{16, 26} though the structure of NEU3 has been investigated using STD NMR.⁴¹ Molecular modeling has been previously used to develop homology models of NEU1-4.^{33, 35, 42, 68, 69} The proposed key residues for each enzyme, based on sequence alignment (**Figure 2**) and site-directed mutagenesis,^{33, 70} are listed in **Table 4**. We docked each of the inhibitors **1–5** in the active sites of the homology models and conducted molecular dynamics (MD) simulations for 100 ns for each system.

Table 4. Key active site residues for hNEU homology models

Enzyme	Catalytic tyrosine	Arginine triad	General acid/base	Other active site residues
NEU1	Y370	R78, R341, R280	E264	H220, T222, E95, R97, D103, L139 ^a
NEU2	Y334	R21, R304, R237	E218	Q270, Y179, Y181, E111, E39, R41, D46, N86
NEU3	Y370	R25, R340, R245	E225	H277, Y179, Y181, E113, E43, R45, D50, N88
NEU4	Y419	R23, R389, R242	E222	W274, Y177, Y179, E111, E41, R43, D48, N86

^a In NEU1, there are no clear homologs to Q270 or E111 (NEU2).

We found that our model of NEU1 was unreliable and likely does not provide significant insight into the active site of this isoenzyme. In simulations with NEU1, only **3** and **5** remained close to the active site of the enzyme; however, the distance between the carboxylate and the nucleophilic tyrosine-OH increased in both cases. In simulations of **3**, this intermolecular distance increased from 5.1 Å after equilibration to 10.9 Å at the end of the simulation, with a maximum distance of 14.4 Å. For **5**, there was a smaller increase from 4.5 Å after equilibration to 7.6 Å at the end of the simulation, with a maximum distance of 10.4 Å. The guanidinium group acts as an anchor during the simulations with **3** and **5**, keeping them in contact with NEU1 for a larger portion of the simulation. The remaining compounds left the active site of NEU1 within 42–58 ns of the simulation. These results led us to conclude that the NEU1 model cannot be used reliably to identify specific protein–inhibitor interactions without further refinement. We observed that all compounds evaluated remained bound to NEU2, NEU3, and NEU4 during the simulations and further details of those simulations are provided below.

3.2.1. Ring conformations

In previous MD simulations with trisaccharide substrates binding to hNEUs, we observed that the Neu5Ac ring remained in ²C₅ conformation in the active site of NEU2 and NEU3.^{2, 71}

However, modifications at the C9 position of the residue could drive the conformation to B_{2,5}. We decided to analyze the ring conformations of free Neu5Ac in these simulations. In the simulation with NEU1, the average conformation of **1** was ²C₅ (see **Table 5**, and Supporting Information), which is the expected solution conformation since the ligand leaves the active site of NEU1 within 44 ns of the simulation. The ring conformation of **1** during simulations with NEU2, NEU3, and NEU4, however, was not ²C₅. Rather, the range of ring conformations varied depending on the isoenzyme. In simulations with NEU2, the ring conformations of **1** spanned a range from ^{4,0}B to ³S₀, with the average at ⁶S₂. With NEU3, the ring conformations of **1** ranged between ⁴S₂ and B_{4,0} for 80% of the simulation and was in the solution conformation, ²C₅, for the remainder of the simulation. For NEU4, the range of ring conformations of **1** was the smallest observed, ^{4,0}B to ^{3,6}B, with the average between ⁴S₂ and B_{2,5}. Presumably, the hydrogen bonds between the carboxylate and the arginine triad compensate for the higher energies of the boat and skew conformers.

Table 5. Average ring conformations of **1–5** during the MD simulations

Compound	NEU1	NEU2	NEU3	NEU4
1 - Neu5Ac	² C ₅	⁶ S ₂	^{3,6} B ^a	⁴ S ₂ /B _{2,5}
2 - DANA	⁶ H ₅	⁶ H ₅	⁶ H ₅	⁶ H ₅
3 - Zanamivir	⁶ H ₅	⁶ H ₅	⁶ H ₅	⁶ H ₅
4 - Oseltamivir	⁴ H ₅	⁴ H ₅	⁴ H ₅	⁴ H ₅
5 - Peramivir	² T ₃ /E ₃	⁴ T ₃	E ₃	⁴ E

^a 80% of the population is ⁰S₃–B_{2,5} conformation, while 20% is in the ²C₅ conformation. See supporting information for more details.

The ring conformation of Neu5Ac in the active site of NEU enzymes has often been observed in boat or skew conformations. A co-crystal structure of the vNEU observed ⁴S₂ and B_{2,5}.⁴⁶ Additionally, Tvaroška and coworkers have run MD simulations of Neu5Ac in solution and bound to the vNEU N1.^{72, 73} While the ²C₅ conformation was the minimum energy conformation in solution, the ^{4,0}B/⁰S₃ conformation was only 2.4 ± 0.4 kcal mol⁻¹ higher in energy. In

simulations in the N1 neuraminidase, differing ring conformations for Neu5Ac were observed depending on which ligand was bound. For free Neu5Ac, the major population was 2C_5 , although there was a minor population at 6S_2 . Taken together, the MD simulations described here, as well as previous work,^{2, 72, 73} demonstrated that sialic acid ring conformation depends both on environment and substitution at the anomeric and N5 positions.

The ring conformation of **2–4** remained the same in all MD simulations, regardless of isoenzyme evaluated (**Table 4**, and Supporting Information). All these compounds contain an endocyclic alkene, which maintains a half-chair conformation when bound to the enzyme or free in solution (as seen in simulations with NEU1). However, as we have previously observed, the conformation of the cyclopentane ring in **5** varies over a range of 180° on the pseudorotational wheel, depending on its environment (**Figure 3** and Supporting Information).⁵⁸ For simulations with NEU1 and NEU3, the conformation of **5** was close to the solution conformation, ${}^2T_3/E_3$ and E_3 , respectively. With NEU2, the average conformation (4T_3) is between solution conformation and that in the crystal structure (2F10);⁴⁸ while with NEU4, the average conformation of 4E is quite similar to that in the crystal structure of NEU2. The flexibility of the ring of **5** allows its functional groups to make different contacts with NEU2, NEU3, and NEU4 as the other compounds (*vide infra*).

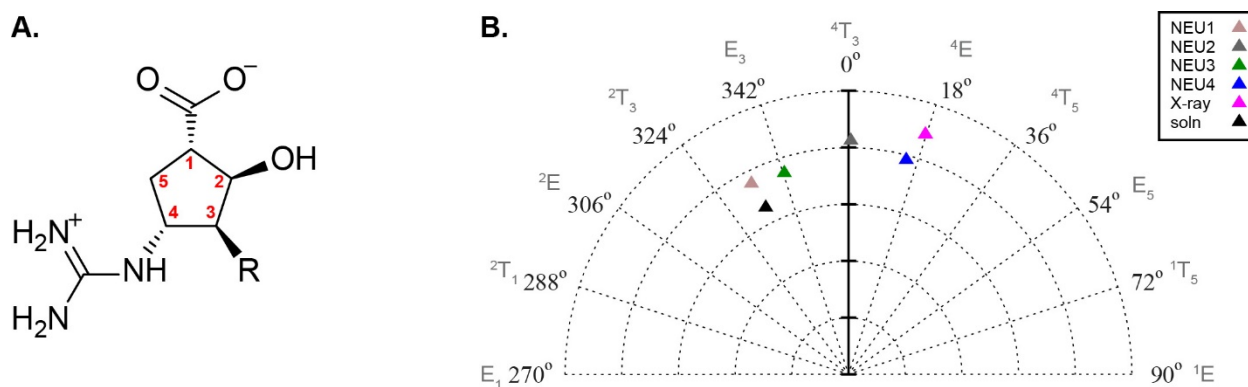


Figure 3. A. The ring atoms of peramivir **5** are numbered the same as our previous study.⁵⁸ B. Average ring conformation of **5** in MD simulations with NEU1 (tan), NEU2 (grey), NEU3 (green), NEU4 (blue). The conformation of **5** from the crystal structure with NEU2 is also shown (magenta, PDB ID: 2F10), as well as the average conformation from solution (black).⁵⁸

3.2.2. Key points of contact between inhibitors and hNEUs

As discussed above, the homology model for NEU1 is inadequate, as such we have limited the discussion here to NEU2, NEU3, and NEU4. Average structures from simulations of compounds **1–5** in the active sites of NEU2, NEU3, and NEU4 shown in **Figure 4–Figure 6**. Ten conformers for each inhibitor relative to the average structure of each hNEU can be found in Supporting Information.

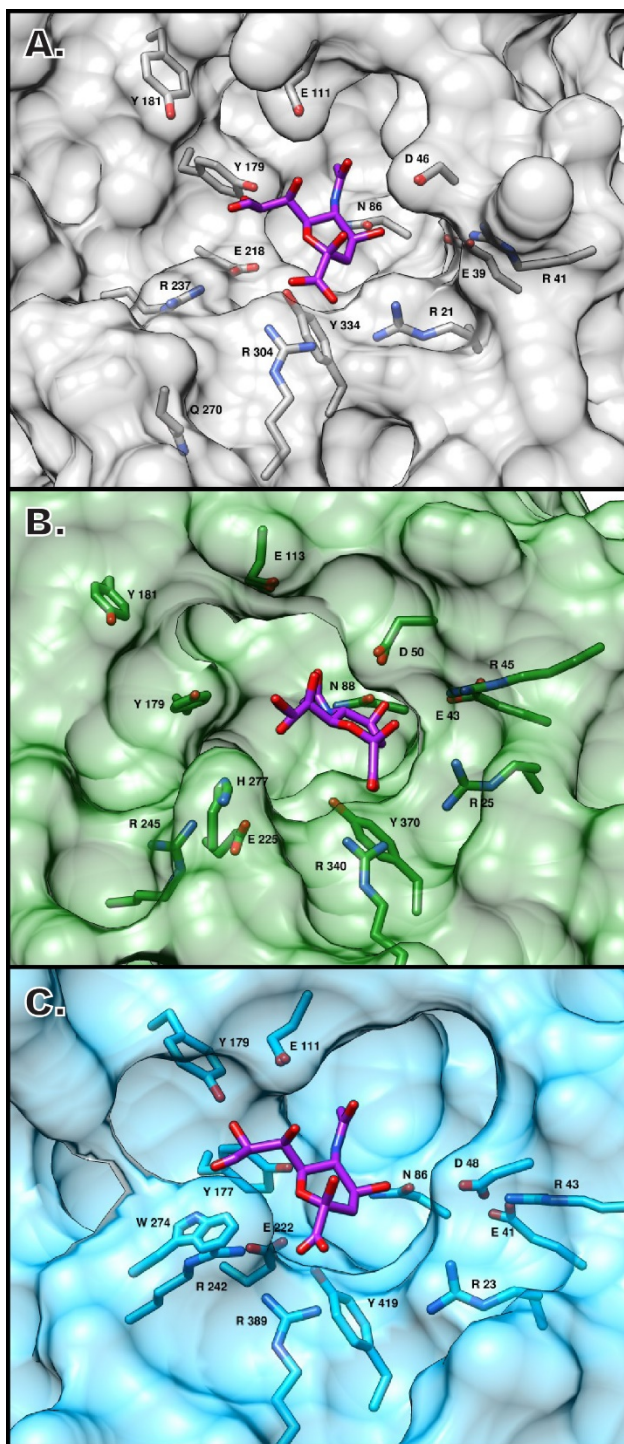


Figure 4. Average structures from MD simulations for Neu5Ac **1** with NEU2 (A.), NEU3 (B.), and NEU4 (C.) **1** is shown in purple, and side chains for key residues are shown, along with the surface representation of the enzymes.

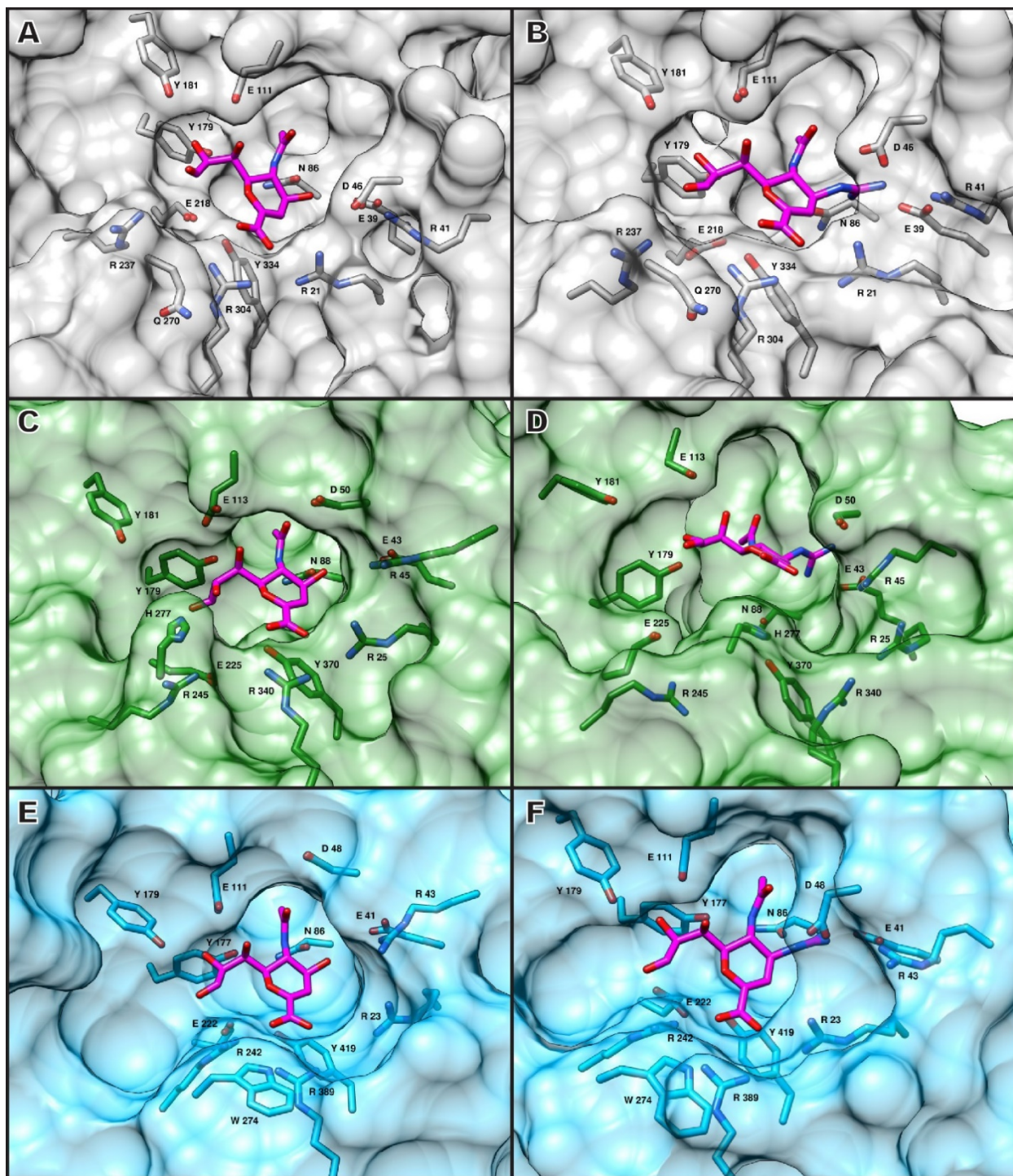


Figure 5. Average structures from MD simulations for DANA **2** and zanamivir **3**. The inhibitors are shown in magenta, and side chains for key residues are shown, along with the surface representation of the enzymes. A. NEU2 with **2**, B. NEU2 with **3**, C. NEU3 with **2**, D. NEU3 with **3**, E. NEU4 with **2**, F. NEU4 with **3**.

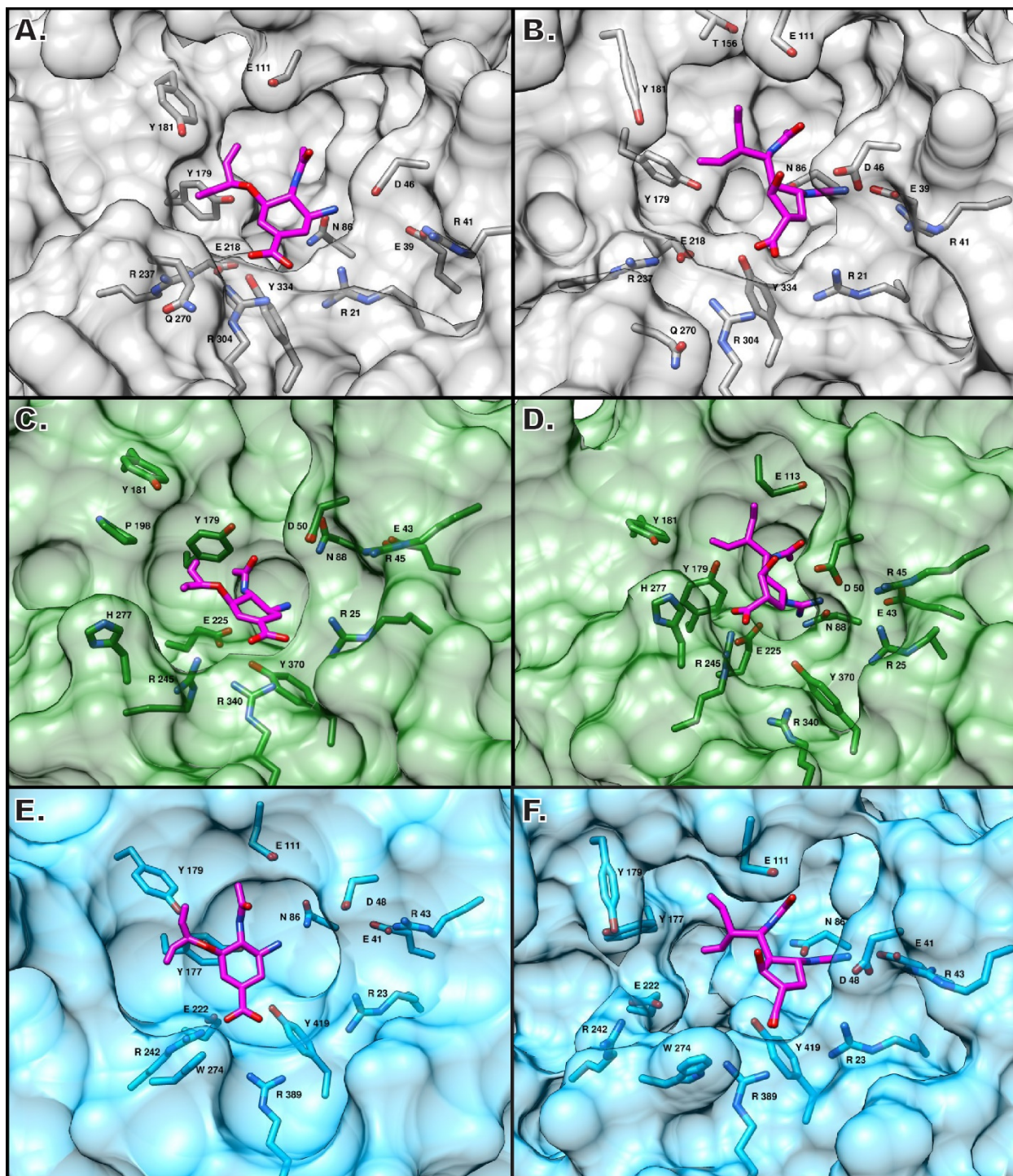


Figure 6. Average structures from MD simulations for oseltamivir **4** and peramivir **5**. The inhibitors are shown in magenta, and side chains for key residues are shown, along with the surface representation of the enzymes. A. NEU2 with **4**, B. NEU2 with **5**, C. NEU3 with **4**, D. NEU3 with **5**, E. NEU4 with **4**, F. NEU4 with **5**.

Compounds **1–5** all contain a carboxylate that forms highly populated (65%–97%) hydrogen bonds to the arginine triad in the active sites of NEU2, NEU3, and NEU4. For most of the simulations, this hydrogen bond is to the central arginine residue – R304 for NEU2, R340 for NEU3, and R389 for NEU4. One exception is the simulation with **3** and NEU3, where **3** is tilted in the active site, exposing the carboxylate to solvent (**Figure 5D**). Consequently, the most populated hydrogen bond between the carboxylate and NEU3 is to Y370 for only 5% of the simulation. Additionally, **5** makes hydrogen bond contacts to a different arginine of the triad – R21 for NEU2 (54%), R245 for NEU3 (81%), and R23 (42%). These hydrogen bonds are also not as populated as those to the carboxylate in the simulations for **1–4**. This difference in hydrogen bond occupancy may be a result of increased ring flexibility in **5**.

Lectins and glycosidases often have shallow active sites, with the hydroxyl groups of carbohydrates displacing ordered water molecules upon binding.⁷⁴ With that in mind, our models retained ordered water molecules observed in the starting crystallography structures that each model was based on (see Sec 2.4.2 for details). In the crystal structure of NEU2 with 3-fluoro-Neu5Ac (4CNS),^{43,44} there are two water molecules in the active site – one in the C4 pocket (HOH 686) and one in the NAc pocket (HOH 515). These solvent molecules remain bound for 84 ns of the simulation of **1** with NEU2, but they leave the active site by 10 ns in the simulation with NEU3 and between 30–48 ns in the simulation with NEU4. Similarly, there is a water molecule in the C4-pocket of the crystal structure of NEU2 with **2** (HOH 395 A, 1VCU).^{26,36} That water molecule remains in the active sites of both NEU2 and NEU3 over the entire simulation with **2**. However, the equivalent water in NEU4 leaves the active site within 68 ns. The C4-pocket of the viral N9 neuraminidase in complex with **4** also contains two water molecules (HOH 1343S and 1349S, 2QWK).^{46,47} These water molecules leave the active sites of NEU2 by 15 ns, NEU3 by 38 ns, and

NEU4 by 21 ns. The guanidinium groups of **3** and **5** take the place of the C4 active-site water in the crystal structure of NEU2 with **2** (compare 1VCU with 2F0Z and 2F10),^{26, 36, 45, 48} and none of the ordered waters from the crystal structures remain in the active sites during any of the simulations with NEU2, NEU3, or NEU4.

The active site waters form water bridges between **1** and NEU2, NEU3, and NEU4 during the MD simulations; specifically, with **1**, E39, and N86 for NEU2 (73%) and with **1**, E41, and N88 and **1** for NEU4 (34%). In NEU3, the corresponding residues were not involved in a water bridge; however, there is a water bridge between **1** and E113 in NEU3 that is populated for 52% of the simulation. This solvent bridge in NEU4 (between **1** and E111) is also seen for 63% of the simulation. In simulations with **2**, the active site waters form solvent bridges among **2**, E39, and N86 in NEU2 (89%); **2**, E43, and N88 in NEU3 (67%); and **2**, E41, and N86 in NEU4 (81%). The C4-hydroxyl in **1** and **2** is replaced by an ammonium in **4**. Hydrogen bonds to solvent dominate this site, but water bridges were less occupied than for **1** and **2** (0%–43%), indicating that the water was less organized around the ammonium group.

While **2** shows inhibitory activity for all four hNEU, **3** is approximately 10-fold selective for NEU2 and NEU3 as compared to NEU4. The guanidinium of **3** takes the place of an active site water in the crystal structure of NEU2 (2F0Z),⁴⁵ and there are hydrogen bonds from the guanidinium to E39 in NEU2 (62%), to E43 in NEU3 (45%), and to E41 in NEU4 (52%), all residues that were involved in water bridges in simulations with **2**. However, the asparagine residues of those solvent bridges do not engage the guanidinium of **3**. Thus, while the guanidinium of **3** occupies a similar space as the active site water in simulations with **2**, the contacts between **3** and the enzymes are not the same as those in the water bridge with **2** and the enzymes. The guanidinium group of **5** forms similar hydrogen bonds in NEU2 and NEU4 – to E39 in NEU2 for

86% of the simulation and to E41 in NEU4 for 99% of the simulation. However, for NEU3, the guanidinium of **5** forms highly populated hydrogen bonds to a different residue, E225 (87%).

Compounds **1–3** contain the glycerol side chain found in the native substrates for hNEUs, and we have observed that changes to this side chain affect selectivity and potency of inhibitors.³⁵ In our MD simulations, hydrogen bonds to solvent dominate these sites with **1**, except for the simulation with NEU4, in which an intramolecular hydrogen bond between HO7 and O1 was populated for 77% of the simulation (**Figure 4C**). In simulations with **2** and **3**, HO7 participates in the most populated hydrogen bonds to the enzymes (38%–80%) – to E111 in NEU2, to E113 in NEU3, and to E111 in NEU4. The other potential hydrogen bonding sites on the glycerol side chain of **2** and **3** are dominated by solvent, apart from the simulation with **3** and NEU4. In that simulation, HO9 forms a hydrogen bond to E222 for 70% of the simulation.

The pentyl side chain of **4** and **5** is known to fit into a hydrophobic pocket in the viral enzymes;^{75, 76} however, it makes contact to mainly polar residues in the simulations between **4** and NEU2, NEU3, and NEU4 (**Figure 6**). In NEU2, the carbon atoms of the pentyl group are closest to (4.2–5.3 Å) the phenolic oxygen of Y181 for 90–98% of the simulation. In NEU3, two of the carbon atoms on the pentyl side chain form a hydrophobic contact to the side chain of P198, but the remaining atoms are close (4.7–5.3 Å) to one of the guanidinium nitrogens of R245 for 68%–100% of the simulation. The simulation with NEU4 is like that of NEU2, the carbon atoms of the pentyl group are closest to (4.3–5.0 Å) the phenolic oxygen of Y179 for 85–99% of the simulation. Many contacts between the pentyl group of **5** are also to polar sites on the enzymes. For NEU2, two carbons in the pentyl group make hydrophobic contact to the γ -carbon of T156, while the remaining carbons in the pentyl group are closest to the phenolic oxygen of Y179 (4.6–5.6 Å) for the entire simulation. For NEU3, three carbons in the pentyl group make hydrophobic contact to

the β -carbon of E113; the remaining carbons in the pentyl group are closest to the phenolic oxygens of Y179 and Y181 (4.2–4.5 Å) for the entire simulation. For NEU4, two carbons in the pentyl group make hydrophobic contact to the γ -carbon of E111; the remaining carbons in the pentyl group are closest to oxygen atoms in Y419 or E222 (4.5–5.3 Å) for the entire simulation.

4 Conclusions

Our experimental determinations of the activity of antiviral compounds **1–5** confirm that these inhibitors have generally poor activity against hNEU.¹⁵ Among these, only zanamivir **3** shows activity in the low micromolar range (primarily for NEU2 and NEU3). We used molecular dynamics and homology modeling of hNEU enzymes to identify features which help explain the low activity of these compounds. Significant features that differ between the viral enzymes and hNEUs include the binding pockets for the glycerol sidechain and the C4 substituent.¹⁶ Furthermore, our results reinforce that the activity of inhibitors designed for the vNEU enzymes against the family of hNEUs cannot be assumed to be identical. In fact, these compounds are generally low in activity against hNEUs, and specifically-designed inhibitors are likely to provide better research and therapeutic avenues.¹⁰

MD simulations identified the glycerol sidechain and C4 binding pockets of hNEU enzymes as recognition elements that were not adequately engaged by vNEU inhibitors. Chavas et al. have previously identified substantial differences in the recognition of the C7–C9 sidechain of Neu5Ac between NEU2 and vNEU.¹⁶ The structure of NEU2 identified E111, Y179, and Y181 residues as coordinating the glycerol sidechain of zanamivir.¹⁶ Furthermore, structures with peramivir bound in the active site of NEU2 showed substantial re-arrangement of these residues. Our MD simulations observed similar changes in the glycerol sidechain binding pocket for NEU3 and NEU4.

Of the 10 wild-type NEU2 crystal structures^{16, 26, 36, 43-45, 48, 77-82} in the Protein Data Bank,⁸³ eight have inhibitors bound, and six of these have an equivalent active site water to the one described above (HOH 395 A in 1VCU).²⁶ The structures with **3**⁴⁵ and **5**⁴⁸ bound lack the active site water, as do the two apo forms.^{26, 77, 78} The active site waters appear to be organized by the ligand. Our MD simulations also support a role for organized water in the C4 pocket of the active sites of NEU2 and NEU3 with DANA, which may help account for the increased potency of zanamivir and derivatives featuring a C4 guanidinium group.³¹ The rigid nature of the guanidinium effectively mimics the organized active site water observed in simulations with DANA and NEU2 and NEU3. The C4 pocket, and the differential activity of zanamivir among hNEUs, suggests that this pocket could be used to provide isoenzyme selectivity. Despite the low potency of antiviral compounds tested here for hNEUs, it is worth noting that the DANA parent scaffold is clearly capable of forming the basis of potent inhibitors. The broad specificity of DANA across species and hNEUs suggests that the scaffold can provide essential contacts in the active site. The DANA scaffold is insufficient alone to provide potent inhibitors, but elaboration has been successful in identifying potent inhibitors for NEU3 and NEU4.^{30, 31}

The MD simulations with NEU1 demonstrate that the homology model is flawed, which is not surprising as NEU1 has the lowest similarity to NEU2 at 22%, compared with 42% similarity between NEU2 and NEU3, and 44% similarity between NEU2 and NEU4. In addition, assays with NEU1 are performed with enriched membrane preparations with cathepsin present, unlike the other three hNEUs that are active in purified form. The homology model of NEU1 may require interactions with members of the complex or a membrane environment to provide predictive results in simulations with **2**. We also ran MD simulations with the NEU1-selective inhibitor C9-

BA²⁹ to further test our homology model (data not shown), and that compound left the active site within 5 ns of the simulation.

The results in the present work support the growing need for additional structural data on other isoenzymes of the hNEU family. While reported structures of NEU2 have been instrumental for the design of new inhibitors, homology models for the remaining isoenzymes are incomplete and, therefore, continue to be a limitation in structure-based design of selective inhibitors. The membrane-associated nature of NEU1, NEU3, and NEU4 is a likely explanation for why these enzymes have not yet been characterized as thoroughly as NEU2. In the absence of well-resolved atomic structures, biochemical, substrate, and inhibitor studies, in combination with other spectroscopic methods, must continue to fill in the gaps in our understanding of the differences between the hNEU isoenzymes.^{41, 65, 68}

5 Abbreviations

4MU-NANA	4-methylumbelliferyl α -D- <i>N</i> -acetylneuraminic acid
DANA	2-deoxy-2,3-dehydro- <i>N</i> -acetylneuraminic acid
GAFF	general AMBER force field
hNEU	human neuraminidase
MBP	maltose binding protein
MD	molecular dynamics
NEU	neuraminidase
Neu5Ac	<i>N</i> -acetylneuraminic acid
SiaT	sialyltransferase
vNEU	viral neuraminidase

6 Acknowledgements:

Funding: This work was supported by the Natural Sciences and Engineering Research Council of Canada (NSERC), the Alberta Glycomics Centre, and the Canadian Glycomics Network.

7 References

1. Varki A. Sialic acids in human health and disease. *Trends Mol Med.* 2008;14(8): 351–360.
2. Hunter CD, Khanna N, Richards MR, et al. Human neuraminidase isoenzymes show variable activities for 9-O-acetyl-sialoside substrates. *ACS Chem Biol.* 2018;13(4): 922–932.
3. Chen X, Varki A. Advances in the Biology and Chemistry of Sialic Acids. *ACS Chem Biol.* 2010;5(2): 163–176.
4. Miyagi T, Yamaguchi K. Mammalian sialidases: Physiological and pathological roles in cellular functions. *Glycobiology.* 2012;22(7): 880–896.
5. Miyagi T, Wada T, Yamaguchi K, Hata K. Sialidase and malignancy: A minireview. *Glycoconjugate J.* 2003;20(3): 189–198.
6. Pshezhetsky AV, Hinek A. Where catabolism meets signalling: neuraminidase 1 as a modulator of cell receptors. *Glycoconjugate J.* 2011;28(7): 441–452.
7. Dridi L, Seyrantepe V, Fougerat A, et al. Positive regulation of insulin signaling by neuraminidase 1. *Diabetes.* 2013;62(7): 2338–2346.
8. Gadhoun SZ, Sackstein R. CD15 expression in human myeloid cell differentiation is regulated by sialidase activity. *Nat Chem Biol.* 2008;4(12): 751–757.
9. Sanders WJ, Katsumoto TR, Bertozzi CR, Rosen SD, Kiessling LL. L-Selectin–Carbohydrate Interactions: Relevant Modifications of the Lewis x Trisaccharide. *Biochemistry.* 1996;35(47): 14862–14867.
10. Cairo CW. Inhibitors of the human neuraminidase enzymes. *MedChemComm.* 2014;5(8): 1067–1074.
11. Von Itzstein M. The war against influenza: discovery and development of sialidase inhibitors. *Nat Rev Drug Discov.* 2007;6(12): 967–974.

12. Gut H, Xu G, Taylor GL, Walsh MA. Structural Basis for Streptococcus pneumoniae NanA Inhibition by Influenza Antivirals Zanamivir and Oseltamivir Carboxylate. *J Mol Biol.* 2011;409(4): 496–503.
13. Xu Z, Von Grafenstein S, Walther E, et al. Sequence diversity of NanA manifests in distinct enzyme kinetics and inhibitor susceptibility. *Sci Rep.* 2016;6: 25169.
14. Walther E, Xu Z, Richter M, et al. Dual acting neuraminidase inhibitors open new opportunities to disrupt the lethal synergism between Streptococcus pneumoniae and influenza virus. *Front Microbiol.* 2016;7: 357.
15. Hata K, Koseki K, Yamaguchi K, et al. Limited Inhibitory Effects of Oseltamivir and Zanamivir on Human Sialidases. *Antimicrob Agents Chemother.* 2008;52(10): 3484–3491.
16. Chavas LMG, Kato R, Suzuki N, et al. Complexity in Influenza Virus Targeted Drug Design: Interaction with Human Sialidases. *J Med Chem.* 2010;53(7): 2998–3002.
17. Albohy A, Mohan S, Zheng RB, Pinto BM, Cairo CW. Inhibitor selectivity of a new class of oseltamivir analogs against viral neuraminidase over human neuraminidase enzymes. *Bioorg Med Chem.* 2011;19(9): 2817–2822.
18. Haxho F, Haq S, Szewczuk MR. Biased G protein-coupled receptor agonism mediates Neu1 sialidase and matrix metalloproteinase-9 crosstalk to induce transactivation of insulin receptor signaling. *Cell Signal.* 2018;43: 71–84.
19. O'Shea LK, Abdulkhalek S, Allison S, Neufeld RJ, Szewczuk MR. Therapeutic targeting of Neu1 sialidase with oseltamivir phosphate (Tamiflu (R)) disables cancer cell survival in human pancreatic cancer with acquired chemoresistance. *Oncotargets Ther.* 2014;7: 117–134.
20. Karhadkar TR, Pilling D, Cox N, Gomer RH. Sialidase inhibitors attenuate pulmonary fibrosis in a mouse model. *Sci Rep.* 2017;7(1): 15069.
21. Amith SR, Jayanth P, Franchuk S, et al. Dependence of pathogen molecule-induced Toll-like receptor activation and cell function on Neu1 sialidase. *Glycoconjugate J.* 2009;26(9): 1197.
22. Li C-Y, Yu Q, Ye Z-Q, et al. A nonsynonymous SNP in human cytosolic sialidase in a small Asian population results in reduced enzyme activity: potential link with severe adverse reactions to oseltamivir. *Cell Research.* 2007;17(4): 357-362.
23. Li J, Van Der Wal DE, Zhu G, et al. Desialylation is a mechanism of Fc-independent platelet clearance and a therapeutic target in immune thrombocytopenia. *Nat Commun.* 2015;6: 7737.
24. Li R, Hoffmeister KM, Falet H. Glycans and the platelet life cycle. *Platelets.* 2016;27(6): 505–511.

25. Liu QP, Hoffmeister K, Sackstein R. Platelet Storage and Reduced Bacterial Proliferation in Platelet Products Using a Sialidase Inhibitor. *Google patents*. US20160000064A1. 2016.
26. Chavas LMG, Tringali C, Fusi P, et al. Crystal Structure of the Human Cytosolic Sialidase Neu2: Evidence for the Dynamic Nature of Substrate Recognition. *J Biol Chem*. 2005;280(1): 469–475.
27. Klepach T, Zhang W, Carmichael I, Serianni AS. ¹³C–¹H and ¹³C–¹³C NMR J-Couplings in ¹³C-Labeled N-Acetyl-neuraminic Acid: Correlations with Molecular Structure. *J Org Chem*. 2008;73(12): 4376–4387.
28. Chong AKJ, Pegg MS, Taylor NR, vonItzstein M. Evidence for a sialosyl cation transition-state complex in the reaction of sialidase from influenza virus. *Eur J Biochem*. 1992;207(1): 335–343.
29. Magesh S, Moriya S, Suzuki T, Miyagi T, Ishida H, Kiso M. Design, synthesis, and biological evaluation of human sialidase inhibitors. Part 1: Selective inhibitors of lysosomal sialidase (NEU1). *Bioorg Med Chem Lett*. 2008;18(2): 532–537.
30. Albohy A, Zhang Y, Smutova V, Pshezhetsky AV, Cairo CW. Identification of Selective Nanomolar Inhibitors of the Human Neuraminidase, NEU4. *ACS Med Chem Lett*. 2013;4(6): 532–537.
31. Guo T, Dätwyler P, Demina E, et al. Selective Inhibitors of Human Neuraminidase 3. *J Med Chem*. 2018;61(5): 1990–2008.
32. Albiñana CB, Machara A, Řezáčová P, Pachel P, Konvalinka J, Kožíšek M. Kinetic, thermodynamic and structural analysis of tamiphosphor binding to neuraminidase of H1N1 (2009) pandemic influenza. *Eur J Med Chem*. 2016;121: 100–109.
33. Albohy A, Li MD, Zheng RB, Zou C, Cairo CW. Insight into substrate recognition and catalysis by the human neuraminidase 3 (NEU3) through molecular modeling and site-directed mutagenesis. *Glycobiology*. 2010;20(9): 1127–1138.
34. Pshezhetsky AV, Potier M. Association of N-Acetylgalactosamine-6-sulfate Sulfatase with the Multienzyme Lysosomal Complex of β -Galactosidase, Cathepsin A, and Neuraminidase: Possible Implication for Intralysosomal Catabolism of Keratan Sulfate. *J Biol Chem*. 1996;271(45): 28359–28365.
35. Zhang Y, Albohy A, Zou Y, Smutova V, Pshezhetsky AV, Cairo CW. Identification of Selective Inhibitors for Human Neuraminidase Isoenzymes Using C4,C7-Modified 2-Deoxy-2,3-didehydro-N-acetylneuraminic Acid (DANA) Analogues. *J Med Chem*. 2013;56(7): 2948–2958.
36. Chavas LMG, Fusi P, Tringali C, et al. Structure of the human cytosolic sialidase Neu2 (PDB ID: 1VCU); 2004. <http://www.rcsb.org/structure/1VCU>. Accessed Jan. 18, 2018.

37. Šali A, Blundell TL. Comparative Protein Modelling by Satisfaction of Spatial Restraints. *J Mol Biol.* 1993;234(3): 779–815.
38. Resource for Biocomputing, Visualization, and Informatics,. UCSF Chimera. candidate version 1.11 ed. University of California, San Francisco (supported by NIGMS P41-GM103311); 2016.
39. Yang Z, Lasker K, Schneidman-Duhovny D, et al. UCSF Chimera, MODELLER, and IMP: An integrated modeling system. *J Struct Biol.* 2012;179(3): 269–278.
40. Pettersen EF, Goddard TD, Huang CC, et al. UCSF Chimera – A visualization system for exploratory research and analysis. *J Comput Chem.* 2004;25(13): 1605–1612.
41. Albohy A, Richards MR, Cairo CW. Mapping substrate interactions of the human membrane-associated neuraminidase, NEU3, using STD NMR. *Glycobiology.* 2015;25(3): 284–293.
42. Magesh S, Suzuki T, Miyagi T, Ishida H, Kiso M. Homology modeling of human sialidase enzymes NEU1, NEU3 and NEU4 based on the crystal structure of NEU2: Hints for the design of selective NEU3 inhibitors. *J Mol Graphics Modell.* 2006;25(2): 196–207.
43. Buchini S, Gallat F-X, Greig IR, et al. Tuning Mechanism-Based Inactivators of Neuraminidases: Mechanistic and Structural Insights. *Angew Chem Int Ed.* 2014;53(13): 3382–3386.
44. Buchini S, Gallat F-X, Greig IR, et al. Human sialidase 2 in complex with 2,3-difluorosialic acid (covalent intermediate) (PDB ID: 4NCS); 2013. <https://www.rcsb.org/structure/4NCS>. Accessed Jan. 18, 2018.
45. Chavas LMG, Kato R, McKimm-Breschkin J, et al. Crystal Structure of the Human Sialidase Neu2 in Complex with Zanamivir Inhibitor (PDB ID: 2F0Z); 2006. <https://www.rcsb.org/structure/2F0Z>. Accessed Jan. 18, 2018.
46. Varghese JN, Smith PW, Sollis SL, et al. Drug design against a shifting target: a structural basis for resistance to inhibitors in a variant of influenza virus neuraminidase. *Structure.* 1998;6(6): 735–746.
47. Varghese JN, Smith PW, Sollis SL, et al. The X-ray Structure of a Complex of 5-N-Acetyl-5-Amino-3-(1-Ethylpropoxy)-1-Cyclohexene-1-Carboxylic Acid (Gs4071) and Wildtype Tern N9 Influenza Virus Neuraminidase (PDB ID: 2QWK); 1998. <https://www.rcsb.org/structure/2QWK>. Accessed Jan. 18, 2018.
48. Chavas LMG, Kato R, McKimm-Breschkin J, et al. Crystal Structure of the Human Sialidase Neu2 in Complex with Peramivir Inhibitor (PDB ID: 2F10); 2006. <https://www.rcsb.org/structure/2F10>. Accessed Jan 18, 2018.
49. wwPDB Foundation. File Format Documentation; <http://www.wwpdb.org/documentation/file-format>. Accessed Feb. 8, 2018.

50. Berman H, Henrick K, Nakamura H. Announcing the worldwide Protein Data Bank. *Nature Struct Biol.* 2003;10(12): 980.
51. Case DA, Berryman JT, Betz RM, et al. AMBER 15. San Francisco, CA: University of California; 2015.
52. Hornak V, Abel R, Okur A, Strockbine B, Roitberg A, Simmerling C. Comparison of multiple Amber force fields and development of improved protein backbone parameters. *Proteins.* 2006;65(3): 712–725.
53. Kirschner KN, Yongye AB, Tschampel SM, et al. GLYCAM06: A generalizable biomolecular force field. Carbohydrates. *J Comput Chem.* 2008;29(4): 622–655.
54. Wang JM, Wolf RM, Caldwell JW, Kollman PA, Case DA. Development and testing of a general amber force field. *J Comput Chem.* 2004;25(9): 1157–1174.
55. Avogadro: an open-source molecular builder and visualization tool. Version 1.1.1, <http://avogadro.openmolecules.net/> ed.; 2012.
56. Hanwell MD, Curtis DE, Lonie DC, Vandermeersch T, Zurek E, Hutchison GR. Avogadro: an advanced semantic chemical editor, visualization, and analysis platform. *J Cheminf.* 2012;4(1): 17.
57. Jakalian A, Bush BL, Jack DB, Bayly CI. Fast, efficient generation of high-quality atomic charges. AM1-BCC model: I. Method. *J Comput Chem.* 2000;21(2): 132–146.
58. Richards MR, Brant MG, Boulanger M, Cairo CW, Wulff JE. Conformational Analysis of Peramivir Reveals Critical Differences Between Free and Enzyme-Bound States. *MedChemComm.* 2014;5(10): 1483–1488.
59. Joung IS, Cheatham TE. Determination of Alkali and Halide Monovalent Ion Parameters for Use in Explicitly Solvated Biomolecular Simulations. *J Phys Chem B.* 2008;112(30): 9020–9041.
60. Jorgensen WL, Chandrasekhar J, Madura JD, Impey RW, Klein ML. Comparison of simple potential functions for simulating liquid water. *J Chem Phys.* 1983;79(2): 926–935.
61. Ryckaert J-P, Ciccotti G, Berendsen HJC. Numerical integration of the cartesian equations of motion of a system with constraints: molecular dynamics of n-alkanes. *J Comput Phys.* 1977;23(3): 327–341.
62. Berendsen HJC, Postma JPM, Gunsteren WFv, DiNola A, Haak JR. Molecular dynamics with coupling to an external bath. *J Chem Phys.* 1984;81(8): 3684–3690.
63. Roe DR, Cheatham TE. PTRAJ and CPPTRAJ: Software for Processing and Analysis of Molecular Dynamics Trajectory Data. *J Chem Theory Comput.* 2013;9(7): 3084–3095.

64. Sandbhor MS, Soya N, Albohy A, et al. Substrate Recognition of the Membrane-Associated Sialidase NEU3 Requires a Hydrophobic Aglycone. *Biochemistry*. 2011;50(32): 6753–6762.
65. Smutova V, Albohy A, Pan X, et al. Structural Basis for Substrate Specificity of Mammalian Neuraminidases. *PLoS ONE*. 2014;9(9): e106320.
66. Seyrantepe V, Landry K, Trudel S, Hassan JA, Morales CR, Pshezhetsky AV. Neu4, a novel human lysosomal lumen sialidase, confers normal phenotype to sialidosis and galactosialidosis cells. *J Biol Chem*. 2004;279(35): 37021–37029.
67. Tringali C, Papini N, Fusi P, et al. Properties of recombinant human cytosolic sialidase hsNeu2 the enzyme hydrolyzes monomerically dispersed GM1 ganglioside molecules. *J Biol Chem*. 2004;279(5): 3169–3179.
68. Rodriguez-Walker M, Daniotti JL. Human Sialidase Neu3 is S-Acylated and Behaves Like an Integral Membrane Protein. *Sci Rep*. 2017;7: 4167.
69. Maurice P, Baud S, Bocharova OV, et al. New Insights into Molecular Organization of Human Neuraminidase-1: Transmembrane Topology and Dimerization Ability. *Sci Rep*. 2016;6: 38363.
70. Wang Y, Yamaguchi K, Shimada Y, Zhao XJ, Miyagi T. Site-directed mutagenesis of human membrane-associated ganglioside sialidase - Identification of amino-acid residues contributing to substrate specificity. *Eur J Biochem*. 2001;268(8): 2201–2208.
71. IUPAC-IUB Joint Commission on Biochemical Nomenclature. Conformational Nomenclature for Five and Six-Membered Ring Forms of Monosaccharides and Their Derivatives. *Eur J Biochem*. 1980;111(2): 295–298.
72. Spiwok V, Tvaroška I. Conformational Free Energy Surface of α -N-Acetylneuraminic Acid: An Interplay Between Hydrogen Bonding and Solvation. *J Phys Chem B*. 2009;113(28): 9589–9594.
73. Raab M, Tvaroška I. The binding properties of the H5N1 influenza virus neuraminidase as inferred from molecular modeling. *J Mol Model*. 2011;17(6): 1445–1456.
74. Lemieux RU. How Water Provides the Impetus for Molecular Recognition in Aqueous Solution. *Acc Chem Res*. 1996;29(8): 373–380.
75. Kim CU, Lew W, Williams MA, et al. Influenza neuraminidase inhibitors possessing a novel hydrophobic interaction in the enzyme active site: Design, synthesis, and structural analysis of carbocyclic sialic acid analogues with potent anti-influenza activity. *J Am Chem Soc*. 1997;119(4): 681–690.
76. Kim CU, Lew W, Williams MA, et al. Structure-activity relationship studies of novel carbocyclic influenza neuraminidase inhibitors. *J Med Chem*. 1998;41(14): 2451–2460.

77. Chavas LMG, Fusi P, Tringali C, et al. Structure of the human cytosolic sialidase Neu2 (PDB ID: 1SNT); 2004. <http://www.rcsb.org/structure/1SNT>. Accessed Jan. 18, 2018.
78. Chavas LMG, Fusi P, Tringali C, et al. Structure of the human cytosolic sialidase Neu2 (PDB ID: 1SO7); 2004. <http://www.rcsb.org/structure/1SO7>. Accessed Jan. 18, 2018.
79. Chavas LMG, Kato R, Mann MC, et al. Crystal Structure of the Human Sialidase Neu2 in Complex with Isobutyl Ether Mimetic Inhibitor (PDB ID: 2F11); 2006. <https://www.rcsb.org/structure/2F11>. Accessed Jan 18, 2018.
80. Chavas LMG, Kato R, Mann MC, et al. Crystal Structure of the Human Sialidase Neu2 in Complex with 3-Hydroxypropyl Ether Mimetic Inhibitor (PDB ID: 2F12); 2006. <https://www.rcsb.org/structure/2F12>. Accessed Jan 18, 2018.
81. Chavas LMG, Kato R, Mann MC, et al. Crystal Structure of the Human Sialidase Neu2 in Complex with 2',3'-Dihydroxypropyl Ether Mimetic Inhibitor (PDB ID: 2F13); 2006. <https://www.rcsb.org/structure/2F13>. Accessed Jan 18, 2018.
82. Buchini S, Gallat F-X, Greig IR, et al. Human sialidase 2 in complex with 2,3-difluorosialic acid (covalent intermediate) (PDB ID: 4NC5); 2013. <https://www.rcsb.org/structure/4NC5>. Accessed Jan. 18, 2018.
83. Westbrook J, Feng Z, Jain S, et al. The Protein Data Bank: unifying the archive. *Nucleic Acids Res.* 2002;30(1): 245–248.